Resolution acuity across the visual field for mesopic and scotopic illumination

Michael O. Wilkinson
School of Optometry, Indiana University, Bloomington, IN, USA
Present address: Premier Research, Inc., Durham, NC, USA

Roger S. Anderson
School of Optometry, Indiana University, Bloomington, IN, USA
Present address: Vision Science Research Group, School of Biomedical Sciences, University of Ulster, Coleraine, UK

Arthur Bradley
School of Optometry, Indiana University, Bloomington, IN, USA

Larry N. Thibos
School of Optometry, Indiana University, Bloomington, IN, USA

We investigated the classical question of why visual acuity decreases with decreasing retinal illuminance by holding retinal eccentricity fixed while illumination varied. Our results indicate that acuity is largely independent of illuminance at any given retinal location, which suggests that under classical free-viewing conditions acuity improves as illumination increases from rod threshold to rod saturation because the retinal location of the stimulus is permitted to migrate from a peripheral location of maximum sensitivity but poor acuity to the foveal location of maximum acuity but poor sensitivity. Comparison with anatomical sampling density of retinal neurons suggests that mesopic acuity at all eccentricities and scotopic acuity for eccentricities beyond about 20° is limited by the spacing of midget ganglion cells. In central retina, however, scotopic acuity is further limited by spatial filtering due to spatial summation within the large, overlapping receptive fields of the A-II class of amacrine cells interposed in the rod pathway between rod bipolars and midget ganglion cells. Our results offer a mechanistic interpretation of the clinical metrics for low-luminance visual dysfunction used to monitor progression of retinal disease.

Introduction

The maxim "to better read a sign, bring the candle closer" was placed on a scientific foundation by the 18th-century astronomer Tobias Mayer, who measured the maximum viewing distance for which stimulus orientation could be correctly identified for a patch of square wave grating illuminated by a candle at a variable distance (Mayer, 1755). By this simple experiment, Mayer discovered that visual acuity (i.e., the highest spatial frequency for which the orientation of the grating could be identified) varied as the sixth root of target luminance over two decades of retinal illuminance, a law of vision that remained uncontested for more than a century (Scheerer, 1987). As shown in Figure 1, Koenig (1897) extended Mayer's power–law relationship to cover the entire six decades of scotopic and mesopic retinal illuminance, a result subsequently confirmed by Shlaer (1937).

Hecht (1928) was the first to ask the mechanistic question of why does acuity vary with illuminance? Hecht accepted Weber's idea that the anatomical basis of spatial resolution of sensory systems is the spacing between neighboring receptive fields (Ross & Murray, 1996; Weber, 1846). Weber believed that the retina was similar to the skin, which he envisioned being covered by an array of discrete touch receptors that formed a mosaic of non-overlapping "sensation circles" (*Empfindungskreise*). Greater spatial density of the mosaic accounts for greater tactile acuity on the fingers, for example, compared to the arms. Similarly, he proposed that sensory circles at the end of optic nerve fibers are more closely spaced in central retina

Citation: Wilkinson, M. O., Anderson, R. S., Bradley, A., & Thibos, L. N. (2020). Resolution acuity across the visual field for mesopic and scotopic illumination. *Journal of Vision*, *20*(10):7, 1–16, https://doi.org/10.1167/jov.20.10.7.

https://doi.org/10.1167/jov.20.10.7 Received July 3, 2020; published October 2, 2020 ISSN 1534-7362

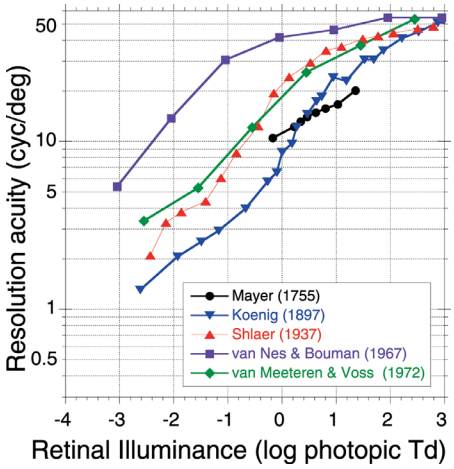

Figure 1. Classical measurements of the dependence of visual acuity on retinal illuminance. We estimated retinal illuminance for Mayer's stimuli by assuming that the intensity of light from his tallow candle was 1 cd and that pupil diameter conformed to the formula of Watson and Yellott (2012).

than in the periphery, which accounts for variation of spatial acuity across the visual field. From that foundation, Hecht reasoned that accounting for the variation of visual acuity with retinal illuminance required variation of functional sampling density, which he suggested might be due to random variation of cone thresholds. As illumination increases, more cones become functional, and thus acuity increases. Although this specific mechanism has been strongly criticized (Walls, 1943; Wilcox, 1932), a convincing alternative explanation remains elusive.

Spatial acuity can also be inferred from the endpoint of contrast sensitivity functions. For example, Van Nes and Bouman (1967) determined contrast sensitivity for detecting a large (4.5° × 8.25°) patch of sinusoidal grating over a wide range of retinal illuminances. They found that detection acuity also increases with retinal illuminance up to 300 trolands (Td), as shown in Figure 1. Subsequently, van Meeteren and Vos (1972) measured contrast sensitivity for resolving a 2.8° × 2.8° patch of sinusoidal grating using an orientation identification task. Their results, also shown in Figure 1, agreed closely with those of Shlaer, confirming a power–law relationship spanning both scotopic and mesopic ranges of illumination.

An important methodological feature of these classical studies was that observers were allowed to change their direction of gaze as the target luminance changed. As every stargazer knows, dim stars are more visible when viewed askance. Thus, as retinal illuminance fell from mesopic to scotopic levels, subjects would have been forced to either change direction of gaze or perhaps shift attention to those parts of the retinal image lying outside the rod-free foveola in order to maintain visibility of a stimulus below the cone threshold (Craik, 1939). But, increasing retinal eccentricity in order to maintain visibility would have reduced acuity because of the foveal-to-peripheral gradient in neural sampling density (Wilkinson, Anderson, Bradley, & Thibos, 2016). In other words, the classical free-viewing paradigm creates a tension between the need for visibility (by increasing eccentricity) and the need for legibility (by decreasing eccentricity). Thus, a potential explanation for the common experience that more light makes better sight is that increased illumination enables the use of more acute retinal locations in a free-viewing situation. This hypothesis predicts that the rate of change in resolution acuity with retinal illuminance would be greatly reduced and perhaps absent entirely if retinal eccentricity were held constant. One of the purposes of the present study was to test this prediction by measuring acuity as a function of retinal illuminance for scotopic and mesopic vision at a series of fixed retinal eccentricities ranging from fovea to far periphery.

The main purpose of our study was to use psychophysical methods to gather behavioral data that would be useful for testing anatomical and physiological hypotheses about the mechanisms that limit visual resolution of gratings at various levels of retinal illuminance located in specific parts of the visual field. A large body of research has led to a modern consensus that retinal sampling by the population of midget retinal ganglion cells is the neural limitation to resolution of high-contrast gratings everywhere in the visual field when retinal illuminance is greater than the cone threshold (for literature review, see Wilkinson et al., 2016). However, that conclusion might not generalize to scotopic vision, because the visual pathway from rods to midget ganglion cells in the mammalian eye includes the A-II class of amacrine cells (Kolb & Famiglietti, 1974), which are less densely packed than midget cells in the central retina of macaque (Wässle, Grünert, Chun, & Boycott, 1995) and human (Lee, Martin, & Grünert, 2019) retinas.

An apparent agreement between quantitative, anatomical predictions of resolution limits imposed by the array of amacrine cells with psychophysical measurements (Lennie & Fairchild, 1994) has led to the conclusion that scotopic acuity in central retina is limited by the coarser A-II amacrine array, whereas scotopic acuity in peripheral retina is limited by the ganglion cell array (Lee et al., 2019; Mills & Massey, 1999; Wässle et al., 1995). This broad generalization is tenuous, however, as it relies on limited psychophysical data obtained at only two levels of retinal illuminance (one near and the other below the cone threshold) and a narrow range of eccentricities (5°–30°) (Lennie & Fairchild, 1994). Moreover, arguments based on sampling theory require evidence that acuity is sampling limited, but Lennie and Fairchild reported

that perceptual aliasing (a definitive sign of neural undersampling) was not observed by their experienced subjects. We have revisited this issue by searching for evidence of neural undersampling over an extended range of conditions covering the full 75° extent of the horizontal temporal visual field for a series of retinal illuminance levels spanning the full 6 log unit range from rod threshold to rod saturation.

The putative functional role of A-II amacrine cells in limiting scotopic resolution acuity also requires clarification. From a signal-processing viewpoint, sampling of the retinal image by an array of retinal neurons limits the fidelity of the discrete neural image in two different ways for two different reasons. The first reason is spatial undersampling of the retinal image, which causes frequency components greater than the Nyquist spatial frequency to be misrepresented as spatial aliases, thereby limiting the neural bandwidth of veridical perception (Wilkinson et al., 2016). Aliasing is an entoptic phenomenon that limits acuity by reducing the *legibility* of test patterns such as gratings or letters (Anderson & Thibos, 1999; Thibos, 1998). The second reason is spatial summation over the receptive field. Just as optical blur reduces contrast in the retinal image, so spatial summation by receptive fields of a sampling array reduces contrast in the neural image of a grating stimulus. Spatial summation is thus a low-pass, spatial-filtering mechanism that attenuates contrast in the neural image, thereby reducing the *visibility* of test patterns regardless of whether the pattern is well sampled or undersampled (Thibos, 2020; Thibos & Bradley, 1995). For a coarse sampling array of neurons with large receptive fields (e.g., the A-II amacrines), this spatial filtering mechanism can potentially reduce resolution acuity to a value less than the Nyquist frequency established by receptive field spacing. To distinguish between these two alternative mechanisms, one based on receptive field spacing and the other based on receptive field size, we investigated the question of does the presumed limitation on scotopic acuity imposed by A-II amacrine cells reduce the legibility or visibility of test stimuli?

Methods

Experimental equipment and procedures were the same as described in our previous report (Wilkinson et al., 2016), but, instead of holding retinal illuminance constant while varying the visual field meridian, in the present experiments we varied retinal illuminance while holding the meridian constant. A circular patch of sinusoidal grating was created on the observer's retina as interference fringes produced by a commercial instrument (Lotmar Visometer; Haag Streit, Berne, Switzerland) (Bradley, Thibos, & Still, 1990; Lotmar, 1972; Lotmar, 1980). We modified the instrument by inserting a 505-nm interference filter in the light path to produce quasi-monochromatic fringes without the bothersome speckle characteristic of lasers. Spatial frequency calibration of the continuously adjustable control was verified theoretically (Thibos, 1990) and empirically (Bradley et al., 1990). Calibration of retinal illuminance produced by this Maxwellian-view instrument was performed by a monochromatic brightness match with a conventional target of the same size. Luminance of the conventional target was then converted to retinal illuminance in trolands by multiplying by pupil area measured during the match. Maximum retinal illuminance produced by the instrument was 540 photopic Td, which was reduced in 1-log-unit steps over a span of 6 log units using neutral-density filters. Stimulus diameter was 1.5° (eccentricity $\leq$ 10°), 2.5° (eccentricity =20°), or 3.5° (eccentricity $\geq$ 30°). These sizes were selected as a compromise to ensure that the patch was large enough to contain at least six cycles of the interference fringes at the acuity limit (Anderson, Evans, & Thibos, 1996) and yet small enough to keep resolution acuity approximately uniform over the retinal patch being stimulated. The test patch was surrounded by a dark field when retinal illuminance was less than 1 photopic Td; otherwise, the stimulus was surrounded by a uniform, white field of the same mean luminance.

The Visometer instrument was mounted on a gimbal that enabled the experimenter to place fringes in the visual field of the observer's right eye up to 75° of eccentricity along the temporal horizontal meridian. A mesopic fixation target seen through a viewing port kept gaze fixed in the primary position, and a bite-bar stabilized the observer's head. For a stimulus at zero eccentricity, the instrument blocked the observer's view of the normal fixation point so in this singular case the observer was instructed to fixate the center of the stimulus. The bite bar was attached to an XYZ linear translator that allowed the experimenter to position the Maxwellian view stimulus in the pupil center, which is essential for avoiding vignetting by the iris. As in our previous experiments, the authors served as observers so that the results reported below may be compared directly with previously published results (Wilkinson et al., 2016). All observers had extensive experience attending to peripheral visual targets while maintaining central fixation and were aware of the importance of steady fixation for achieving the purpose of this investigation. Learning to suppress the natural tendency to fixate peripheral stimuli was aided by the futility experienced when attempting to fixate a peripheral stimulus that disappeared (due to vignetting by the iris) when ocular rotations toward the stimulus displaced the eye's pupil away from the instrument's optical axis. Neither cycloplegia nor spectacle correction was required, as the contrast of interference fringes is not

affected by defocus or astigmatism (Halliday & Ross, 1983; Le Grand, 1937).

Sampling-limited measures of visual resolution acuity were obtained by a descending method of adjustment. The experimenter set fringe frequency well above the resolution limit and then set orientation to one of four possible settings (0° = horizontal, 90° = vertical, 45° = right oblique, 135° = left oblique). The subject's task was to reduce fringe frequency continuously until grating orientation could be identified with confidence. This paradigm gives highly repeatable results, because when fringe frequency is above the resolution limit the stimulus appears as an unstable perceptual alias with random variations in spatial frequency, orientation, and structure (Thibos & Bradley, 1993; Thibos, Walsh, & Cheney, 1987). When spatial frequency transitions from this non-veridical, aliasing zone of the spectrum into the veridical zone, perceptual stability is achieved and stimulus orientation can be identified with few errors. This criterion of temporal stability also avoids supra-Nyquist performance that can occur for forced-choice orientation identification for irregular sampling arrays (Evans, Wang, Haggerty, & Thibos, 2010). A pilot experiment in peripheral retina for two of our subjects indicated that resolution values obtained by method of adjustment were approximately 10% less than the spatial frequency that yielded 75% correct responses on a two-alternative forced-choice paradigm. Twenty resolution settings (five each for four orientations: 0°, 45°, 90°, and 135°) were obtained for every combination of visual field location and retinal illuminance. Observers were allowed unlimited viewing time, as slow adjustment of the spatial frequency of the grating was encouraged to reduce intertrial variability. Bracketing adjustments, an often used method of adjustment, were not allowed to preserve orientation identification as a perceptual veridicality task. At the end of each session, the experimenter recorded comments from the observer regarding subjective perception of the entoptic aliasing phenomenon.

The absolute visual threshold for the Visometer stimulus was measured for each subject by setting the spatial frequency of the interference fringes to a high value well beyond detection acuity so the stimulus appeared to be a uniform field when viewed peripherally. A preliminary experiment conducted at 30° eccentricity indicated that 30 minutes of dark adaptation reduced the threshold for detecting the stimulus field to approximately –3.5 to –4.0 log scotopic Td for all three observers, a range similar to absolute threshold values reported previously (Walraven, Enroth-Cugell, Hood, MacLeod, & Schnapf, 1990). Based on that result, visual acuity measurements began with test illuminance of –2.5 log scotopic Td (approximately 1 log unit above the absolute rod threshold) and incremented (by removing neutral-density filters) in 1-log-unit steps to a maximum of +3.5 log scotopic Td. Because this maximum value lies in the expected range of rod saturation (+3.3 to +3.7 log scotopic Td) (Aguilar & Stiles, 1954), our experimental design covered the entire scotopic and mesopic domain of human vision. The testing sequence was from dim to bright illumination at a given retinal locus before eccentricity was changed, and the process was repeated until data had been collected across the full extent of the horizontal nasal retina (0°, 2.5°, 5°, 10°, 20°, 30°, 40°, 50°, 60°, and 75° of eccentricity in the temporal visual field). One observer (LT) was tested for all combinations of retinal eccentricities and illuminances, whereas some combinations were eliminated from the testing of the other observers (AB, RA).

Four auxiliary experiments were required to fully interpret the results of the main experiment described above. The first auxiliary experiment employed the method of constant stimuli to measure performance for detection and for resolution of gratings for natural viewing of scotopic stimuli. The grating appeared inside a circular window (3.5° in diameter located 30° in the temporal visual field) displayed on a computer monitor 2.5 m from the subject's right eye. The left eye was covered with a filter that was opaque to visible wavelengths but transparent to infrared radiation, which enabled measurement of pupil diameter under experimental conditions. The pupil diameter of the tested eye was assumed to be the same as that of the fellow eye and was measured with the aid of night-vision goggles (military specification, third generation, image intensifier tube with photon gain = 25,000). The grating stimulus was surrounded by a uniform field of the same mean luminance, and a fixation point 2.5 m from the subject controlled gaze and accommodation. Refractive error at the peripheral stimulus location was corrected with spectacle lenses prescribed by a subjective technique that optimizes contrast sensitivity for detection of high spatial frequency gratings (Wang, Thibos, Lopez, Salmon, & Bradley, 1996).

Detection performance was measured with a two-interval forced-choice (2IFC) paradigm in which the observer's task was to discriminate a horizontal grating of high contrast from a uniform field. Resolution performance was measured with a two-alternative forced-choice paradigm (2AFC) in which the observer's task was to identify the orientation of the grating (horizontal or vertical). Performance for these two orientations was tracked separately, but only the results for horizontal gratings are reported for this auxiliary experiment because they provide the more stringent test. Sampling-limited acuity is typically greater for radial (i.e., horizontal) gratings than for tangential (i.e., vertical) gratings (Anderson, Wilkinson, & Thibos, 1992; Wilkinson et al., 2016), so if a grating generates aliasing when horizontal it will also generate aliasing when vertical. For both paradigms, a selection of seven

spatial frequencies was randomly interleaved and a minimum of 20 trials per condition were conducted, resulting in at least 140 (2IFC) and 280 (2AFC) trials in the experiment.

For the second auxiliary experiment, a more efficient staircase procedure was used to implement the 2IFC and 2AFC paradigms using the same apparatus described above. Neutral-density filters were used to vary target luminance over the 6-log-unit range of scotopic plus mesopic illumination levels for a target at fixed eccentricity (30°). Pupil diameter of the tested eye was assumed to be the same as that of the fellow eye as measured with infrared radiation.

In the third auxiliary experiment, we measured the absolute threshold for rod and cone vision using a conventional dark-adaptation paradigm for detecting 505-nm light filling a circular test spot of diameter 1.5° (at 0° and 10° eccentricity) or 3.5° (at 30° and 50° eccentricity). For this purpose, it was convenient to use the patch of interference fringes produced by the Lotmar instrument as the stimulus, set to a high spatial frequency (60 cpd) beyond the cutoff frequency for visibility of aliasing at all eccentricities. Following exposure to a pre-adapting field of luminance of 7300 cd/m^2, the threshold was measured initially for a space-averaged test luminance of 0.75 cd/m^2 and then followed sequentially as the test luminance was decreased in 0.2-log-unit steps. Measured pupil size was 7 mm throughout the measurement phase.

The fourth auxiliary experiment gave an independent estimate of the cone threshold by measuring the Purkinje shift at 0° and 30° eccentricity. A uniform field displayed on a color cathode-ray tube monitor alternated at 12 Hz between red and green light or between yellow and blue light. The subject adjusted the relative luminance of the two colors to minimize subjective flicker for a sequence of retinal illuminance levels spanning the same 6-log-unit range as in the main experiment. Pupil diameter was assumed to be the same as in the first auxiliary experiment for the purpose of computing retinal illuminance from target luminance.

Results

Resolution acuity is defined in this report as the highest spatial frequency supporting veridical perception of orientation for sinusoidal gratings. Resolution acuity varied slightly with grating orientation, so we report in Figure 2 the average across orientation to provide a representative value. Because five acuity settings at each of four target orientations were obtained for every stimulus condition, we had 20 measurements available for computing acuity statistics. Standard deviation of the 20 settings was typically 5% to 10% of the mean, independent of retinal location or retinal illuminance. The standard errors of the mean are thus smaller than the radius of the symbols plotted on a logarithmic ordinate (Figure 2), which demonstrates the high level of precision achieved by our practiced observers and confirms that stimulus diameter was small enough to ensure homogeneity of the retinal sampling array and that fixation was sufficiently precise. The loss of acuity with stimulus eccentricity was remarkably similar for all three subjects at every level of retinal illuminance, which we take as evidence of accurate fixation. The largest standard error of the mean across subjects for any test condition was less than the symbol diameter used in the lower right panel of Figure 2 showing the mean across subjects. Tabulated data used to create Figure 2 are provided in Supplementary Materials.

For all observers, acuity was nearly identical for the three highest levels of retinal illuminance tested (+2.73, +1.73, +0.73 log photopic Td) at every eccentricity. The first clear indication that reducing retinal illuminance reduces acuity at any fixed retinal location occurred near the cone threshold for the –0.27 log photopic Td stimuli. When retinal illuminance was reduced another log unit to –1.27 log photopic Td, performance of the task was no longer possible at the fovea because the stimulus was not visible. Thus, based on this experiment, the foveal cone threshold lies somewhere between –0.27 and –1.27 log photopic Td. As retinal illuminance was further reduced, acuity declined more in central than in peripheral retina.

Perhaps the most interesting feature of Figure 2 is the steady migration of peak acuity away from the fovea to the parafovea (2.5° to 5°) for stimuli approximately 1 log unit below the foveal cone threshold, with further migration into the periphery (10°) for retinal illuminance approximately 2 log units below the foveal cone threshold. Another notable feature of the results is the small dip in the scotopic curves at 20° eccentricity, possibly due to the "rod gulley," a local dip in rod density where the ring of high rod density crosses the horizontal meridian (Curcio, Sloan, Kalina, & Hendrickson, 1990). Alternatively, the dip might be due to partial overlap of the stimulus and the blind spot, centered at 15° to 16° eccentricity for our subjects (Wilkinson et al., 2016), but that seems unlikely because the dip was only evident for scotopic illuminances. These features were evident for all three observers and therefore were also present when the data were averaged across observers.

In addition to the quantitative data displayed in Figure 2, subjects were asked to report any entoptic perceptions of aliasing, the subjective manifestation of neural undersampling. All three subjects reported subjective aliasing for high spatial frequencies for all but the lowest illumination level and for all eccentricities greater than 10°. The only consistent exception to this general result was that aliasing was not reported by

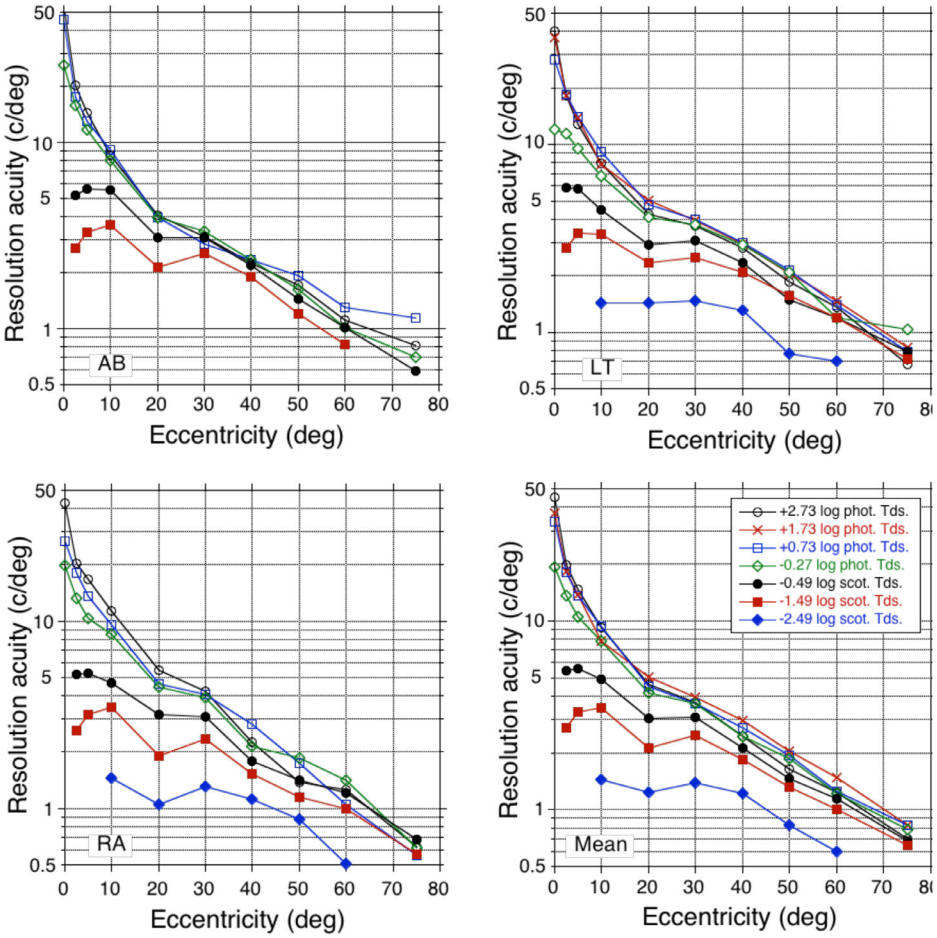

Figure 2. Variation of resolution acuity across the visual field for a range of retinal illuminances. Symbols indicate the mean of 20 measurements (five replications at each of four grating orientations). Standard errors of the mean were smaller than the radius of the symbols plotted on a logarithmic ordinate. Individual panels show results for three observers, and the mean acuity across subjects is shown in the bottom right panel. The symbol legend for the mean data also applies to individual observers. Retinal illuminance is specified in photopic trolands for the four highest levels of retinal illuminance and in scotopic trolands for the three lowest. The tabulated data used to create these graphs are provided in Supplementary Materials.

any of the subjects for eccentricities between 2.5° and 10° for the three dimmest illumination levels tested (–0.73 to –2.73 log photopic Td). Acuity was greatest for horizontally oriented gratings at all but the lowest illuminance level tested, as reported previously for these same observers for high-mesopic stimuli (Anderson et al., 1992; Wilkinson et al., 2016). Subjects commented that the oblique gratings tended to alias more in orientation whereas the radial and tangential gratings aliased more in spatial frequency.

To quantify the tendency for acuity to be greater for radially oriented gratings, we computed orientation bias at each test location in the visual field using the vector-summation formula given in figure 1B of Wilkinson et al. (2016). Bias is a normalized, unitless vector with length indicating the magnitude of bias on a scale of 0 (no bias) to 1 (total bias) and direction indicating the preferred fringe orientation for maximum acuity, with 0° indicating radially oriented gratings. As shown in Figure 3A, the average magnitude of orientation bias computed for the combined population of subjects and retinal illuminance values tended to increase with retinal eccentricity (Wilkinson et al., 2016). This dependency was much the same when the population averages were computed separately for mesopic or scotopic values of retinal illuminance. As shown in Figure 3B, preferred grating orientation tended to be within ±25° of horizontal (i.e., radial preference for stimuli located on the horizontal meridian), which is consistent with exponential radial stretching of the retinal sampling mosaic (Thibos, 2020; Wilkinson et al., 2016).

To better visualize differences between scotopic and mesopic acuity, the data presented in Figure 2 are replotted in Figure 4 with a format that reveals more directly the effect of retinal illuminance on resolution

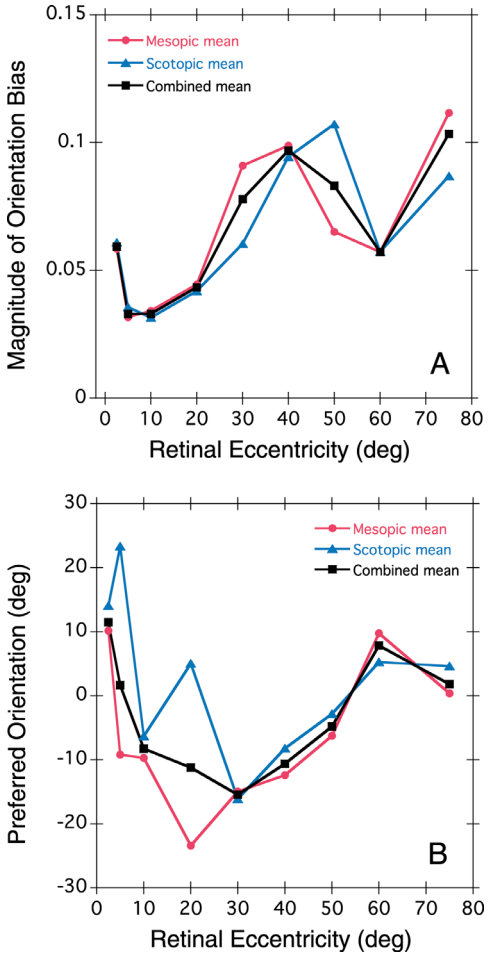

Figure 3. Orientation bias of resolution acuity as a function of retinal eccentricity averaged across subjects and retinal illuminance. (A) Magnitude of orientation bias. (B) Preferred stimulus orientation relative to the radial (i.e., horizontal) orientation. Symbols show the population mean computed separately for mesopic or scotopic test luminance or for the combined dataset including all test luminances.

acuity when retinal eccentricity is held constant. As noted above, standard errors of the mean for individual observers and for the mean performance across observers were typically smaller than the symbols used to display the data. Retinal illuminance had little effect on acuity in the peripheral field beyond 30° or for more central field locations when illuminance exceeded 0 log photopic Td. Thus, the largest effect of illuminance occurred for scotopic stimuli in the central visual field where the curves sloped downward and terminated near the absolute rod threshold of visibility.

The auxiliary experiments

The scotopic, mesopic, and photopic regions of vision are defined according to whether rods alone, rods and cones, or cones alone operate (Stockman & Sharpe, 2006). Categorizing the illumination levels used in our experiments required estimates of rod and cone thresholds at various eccentricities, which we made in two ways, as described next. We also wished to substantiate subjective reports of aliasing with objective evidence obtained by two other auxiliary experiments described at the end of this section.

Cone thresholds were measured at four eccentricities for subject LT using the classic dark-adaptation paradigm (Hecht, Haig, & Wald, 1935). Examples of the time course of the visual threshold at two retinal eccentricities following an intense adapting light are shown in Figure 5. Exponential functions fit separately to the fast (cone) and slow (rod) segments were used to quantify thresholds (Rushton, 1965). The cone plateau, established after 5 to 10 minutes of dark adaptation yielded cone thresholds of –1.0, –0.3, –0.3, and –0.2 log photopic Td for the eccentricities of 0°, 10°, 30°, and 50°, respectively. Corresponding rod thresholds were –2.3, –2.4, –3.6, and –4.0 log photopic Td or –1.5, –1.6, –2.8, and –3.2 log scotopic Td. Stimulus sizes for this auxiliary experiment were the same as for the main experiment, so these results may be compared directly with the individual curves in Figure 4. Because the 0° eccentricity stimulus (1.5° diameter) was slightly larger than the expected rod-free area of the fovea (0.7°–1.4° diameter) (Curcio et al., 1990), we presume that a rod threshold measured at 0° eccentricity refers to the retinal location just outside the all-cone foveola (Osterberg, 1935).

Measurements of the Purkinje shift provided an independent confirmation of cone thresholds inferred from Figure 5 for the same subject (LT) at 0° and 30° eccentricity. Based on a minimum-flicker criterion, the relative luminance of red and green light required to equate their perceived brightness is shown in Figure 6 as a function of retinal illuminance. As expected for predominantly rod-free vision, a Purkinje shift did not occur for foveal viewing (i.e., the ratio of red and green luminances required to minimize flicker was independent of retinal illuminance). In peripheral vision, however, the red/green ratio changed as the balance between rod and cone input to visual perception of brightness shifted. For the brightest stimulus tested, the red/green ratio at 30° eccentricity was the same as for the fovea, indicating that cones dominated rods. As the stimulus luminance declined, the ratio increased because rods began to dominate. At the cone threshold (plateau of –0.3 log Td at 30°, according to Figure 5), the red/green ratio had increased nearly tenfold and remained constant at that value as retinal illuminance decreased further. A similar result was obtained when the experiment was repeated using yellow and blue lights. These results are consistent with Purkinje's shift in wavelength of peak sensitivity from 507 nm to 555 nm as retinal illuminance varies across the mesopic range

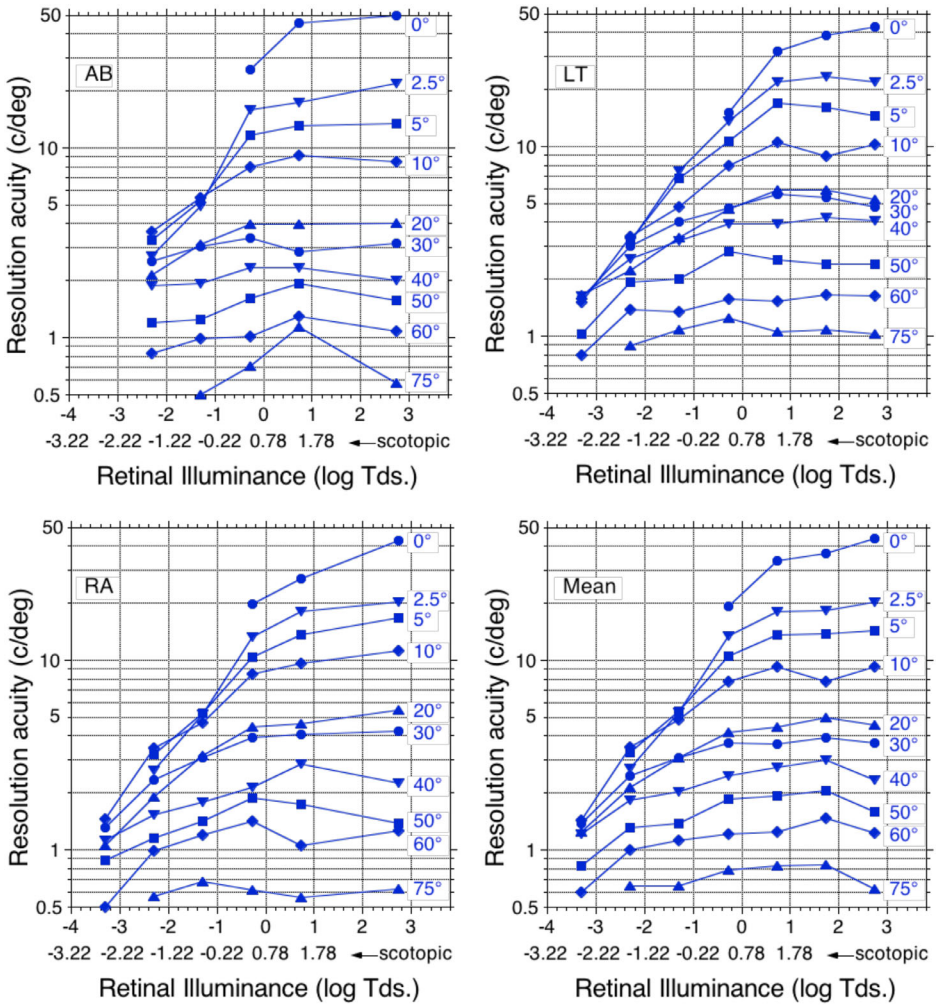

Figure 4. Effect of retinal illuminance on resolution acuity depends on retinal eccentricity. Symbols show the same data as in Figure 2, with individual panels showing results for three observers, and the mean across subjects is shown in the bottom right panel. Numbers next to each dataset indicate retinal eccentricity in the temporal visual field. Retinal illuminance is specified in photopic trolands in the upper abscissa labels and in scotopic trolands in the lower abscissa labels.

from cone threshold to rod saturation (Stockman & Sharpe, 2006). On the basis of these results, we adopted the cone thresholds measured in the dark adaptation experiment as the border between rod-only scotopic vision and mixed rod and cone mesopic vision for the purpose of interpreting the data displayed in Figure 4.

To substantiate the subjective reports of aliasing described above in connection with Figure 2, two auxiliary experiments were performed for representative conditions. The first employed the method of constant stimuli to measure frequency-of-seeing psychometric functions for detecting and for resolving gratings for natural viewing of scotopic stimuli displayed on a computer monitor. The results of the experiment for retinal illuminance well below the cone threshold (–0.9 log scotopic Td) are shown in Figure 7 for observer RA. The horizontal separation between the curves for resolution and the detection tasks is the aliasing zone that signifies neural undersampling of stimuli for which grating contrast is detectable. For comparison, resolution acuity for interference fringes at this eccentricity (2.8 cpd, interpolated from the data in Figure 4) is shown by the dashed vertical line. This line intersects the resolution psychometric function at the corner frequency where performance began to fall below 100%. This result is to be expected, as the subject's task for method of adjustment in the main experiment was to find the maximum spatial frequency for which perception remained veridical.

The width of the aliasing zone was found to vary with retinal illuminance in a second auxiliary experiment performed at a fixed retinal locus (30° eccentricity). The results of that experiment are displayed in Figure 8 for the same subject (RA) as in Figure 7. Detection acuity exceeded resolution acuity for retinal illuminance values

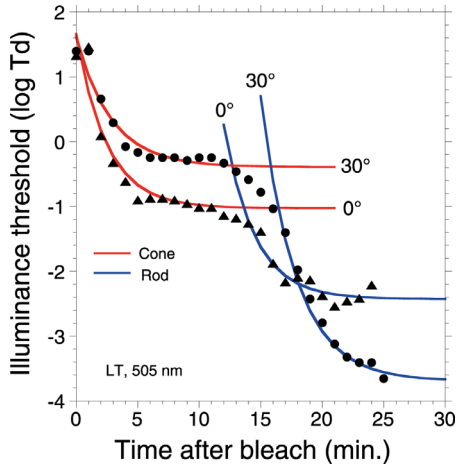

Figure 5. Dark-adaptation functions for two retinal eccentricities (0° and 30°). Symbols show empirical measurements, smooth curves show exponential functions fit to the rod and cone portions of the data. Absolute thresholds for cones and rods at a given retinal location are equal to the ordinate values of the plateau portions of the corresponding curves. Subject LT, 505-nm light.

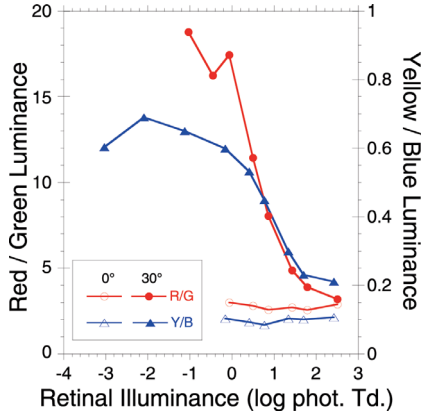

Figure 6. Confirmation of cone threshold using the Purkinje shift paradigm. Symbols show the ratio of red to green or yellow to blue luminances required to minimize perceived flicker at two eccentricities (0° and 30° in temporal visual field). Subject LT.

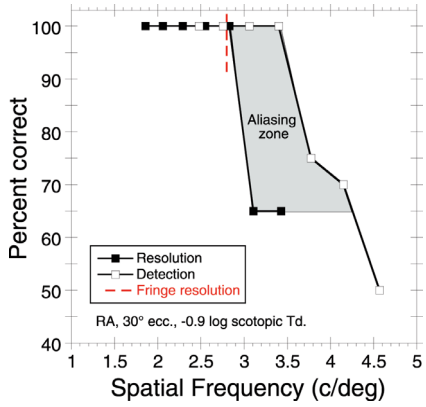

Figure 7. Psychophysical evidence of sampling-limited resolution of gratings in scotopic peripheral vision (30° eccentricity). Symbols show performance in forced-choice experiments for natural viewing of gratings displayed on a computer monitor. The dashed vertical line indicates resolution acuity for interference fringes according to Figure 4. The horizontal extent of the aliasing zone indicates the range of spatial frequencies for which gratings were visible but not resolvable. Subject RA.

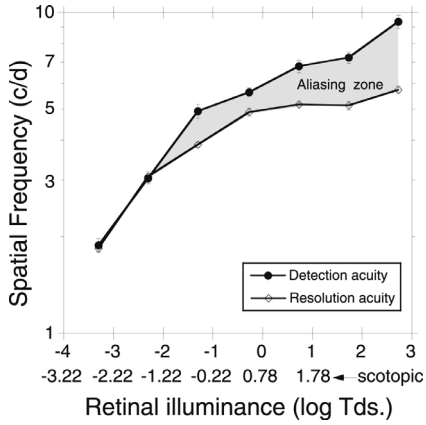

Figure 8. Objective demonstration that the width of the aliasing zone varies with retinal illuminance in peripheral vision. Symbols show detection acuity and resolution acuity determined with a forced-choice staircase paradigm for natural viewing of gratings displayed on a computer monitor (30° eccentricity). Error bars indicate standard errors of the mean values of seven staircase reversals. The vertical extent of the aliasing zone indicates the range of spatial frequencies for which gratings were visible but not resolvable. Data are for the same observer (RA) as in Figure 7.

greater than –1.5 scotopic Td. The vertical separation of the two curves in this figure is the aliasing zone, which is seen to extend below the cone threshold, well into the scotopic range of rod-only vision.

To summarize our findings, the panel of Figure 4 showing the average effect of retinal illuminance on resolution acuity for our three observers is augmented in Figure 9 with measurements of cone and rod thresholds obtained from the dark-adaptation auxiliary experiment of Figure 5. The cone threshold, which varied slightly with eccentricity for our stimulus, partitions the span of retinal illuminance into scotopic and mesopic zones. Rod saturation, which demarcates the border between mesopic and photopic vision, was not determined for our subjects but is expected to lie near the maximum illuminance tested (3.5 log scotopic Td) (Aguilar & Stiles, 1954). A major feature of Figure 9 is that, for all retinal locations outside the fovea, mesopic acuity is nearly independent of retinal

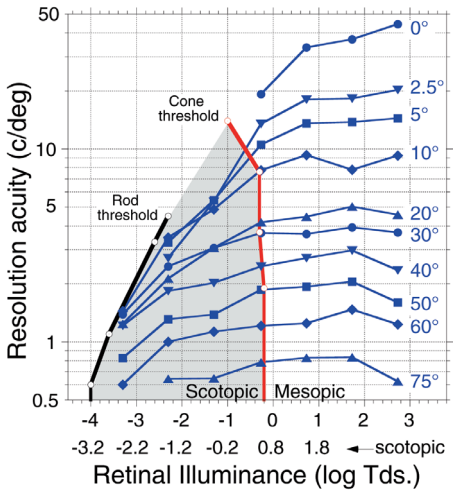

Figure 9. Summary of mean acuity results overlaid with the empirically determined scotopic and mesopic zones of retinal illumination. Red circles indicate cone thresholds (and the interpolated acuity at cone threshold) at four eccentricities. The solid red line connecting the red circles indicates the border between scotopic and mesopic vision. Black circles indicate rod thresholds (and extrapolated acuities for rod vision) at the same four eccentricities (0°, 10°, 30°, and 50°). The solid black line connecting the black circles indicates the lower border of the scotopic zone. The upper border of the mesopic zone, determined by rod saturation, is expected to be located near the highest retinal illuminance tested (3.5 log scotopic Td).

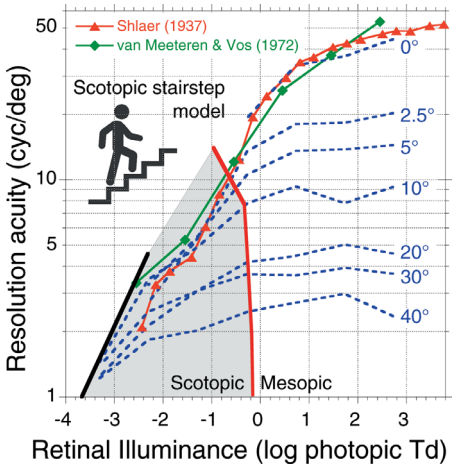

Figure 10. Comparison of current results with classical measurements of visual acuity for free viewing of gratings of variable retinal illuminance. The symbol key for the classic studies is the same as in Figure 1. Dashed lines show data from Figure 4 for eccentricities in the range 0° to 40°. Free-viewing acuity values reported by Shlaer (1937) and by van Meeteren and Vos (1972) are nearly identical and closely follow the envelope of curves for fixed stimulus eccentricities. The scotopic stairstep model is a conceptual analog of the graph of a family of dashed curves displaying visual acuity as a function of retinal illuminance for a multitude of retinal eccentricities.

illuminance. This result is consistent with the subjective reports of aliasing, which we take as evidence that peripheral resolution acuity of high-contrast gratings is sampling limited throughout the mesopic zone. If sampling is the limiting mechanism, then we must reject the competing filtering hypothesis (see Introduction) that spatial summation across the receptive fields of individual neurons limits resolution acuity by limiting visibility of the grating. For scotopic stimuli beyond 30° eccentricity, a significant loss of acuity occurred only when illuminance was within 1 log unit of the absolute rod threshold, suggesting that neural sampling is also the limiting mechanism for peripheral scotopic acuity. Central scotopic acuity is a notable exception to these generalizations. For eccentricity $< 30°$, individual data curves have positive slope in the scotopic zone, a feature discussed at length below.

Discussion

Why does more light make better sight?

One purpose of our study was to test a potential explanation for the common experience that more light makes better sight, an observation that likely predates written history when cave-dwelling artists painted ancient figures by torchlight. All of the classic scientific reports from the 18th to 20th centuries reviewed in Figure 1 emphasized a large, monotonic increase of acuity with retinal illuminance. To account for this phenomenon, we hypothesized that, when retinal illumination is reduced below the foveal cone threshold, observers adopt a strategy of manipulating gaze (or attention) to observe the stimulus when located at the optimum retinal locus for maximizing acuity, given the available level of retinal illumination. By this account, the classical free-viewing paradigm creates a tension between the need for visibility (by *increasing* eccentricity to increase rod density) and the need for legibility (by *decreasing* eccentricity in order to increase neural sampling density). To test this idea, we measured the effect of retinal illuminance on visual acuity under scotopic and mesopic conditions while fixing gaze to allow controlled placement of the stimulus image at known retinal locations. Our results (Figure 9) are compared in Figure 10 with those from classical studies (Figure 1). For this purpose we excluded the data from Mayer (1755) and from Koenig (1897) because of our concern that conversion of antiquated photometric units that depended on assumptions regarding pupil size may have produced erroneous estimates of retinal illuminance. We also excluded the abnormally high

acuity values inferred from contrast sensitivity functions published by Van Nes and Bouman (1967) on the grounds that their observers probably used a detection criterion rather than a resolution criterion. As shown in Figure 8 and described previously (Thibos, Still, & Bradley, 1996), detection acuity is typically greater than resolution acuity in peripheral vision. Thus, we concentrate our attention in Figure 10 on acuity values reported by Shlaer (1937) and by van Meeteren and Vos (1972), which are nearly identical. We justify the direct comparison of acuity obtained with interference fringes (which do not suffer contrast attenuation by optical aberrations of the eye) with natural viewing of conventional stimuli (without optical correction of refractive errors) on the grounds that resolution acuity for sinusoidal gratings is sampling limited, not contrast limited. Even large focusing errors have no effect on peripheral resolution acuity for high-contrast stimuli (Anderson, 1996; Wang, Thibos, & Bradley, 1997).

The main insight gained from Figure 10 is that free-viewing acuity closely follows the envelope of the family of acuity curves for the specific eccentricities we reported in Figure 4. The envelope in this context refers to the locus of maximum acuity values attainable for each value of retinal illuminance. In the mesopic zone, maximizing acuity under free-viewing conditions is achieved by foveal viewing. However, in the scotopic zone, maximum acuity for a given level of retinal illuminance is achieved by adjusting gaze to create an eccentric viewing angle specified by the envelope. Thus, the evidence of Figure 10 compels us to suggest that subjects in these previous experiments employed a fixation strategy that optimized resolution.

The logic of our argument is conveyed graphically by the scotopic stairstep model shown in the inset of Figure 10. The height of each step above ground level indicates sampling-limited visual acuity, and the horizontal location of each tread in the staircase indicates retinal illuminance of a grating to be resolved. Using a more clinical metaphor, we might call this staircase an acuity hill of vision terraced with acuity isopters of retinal illuminance. Now consider an agent responsible for placing the visual stimulus at that retinal location for which visual acuity is highest. If retinal illuminance is near the rod threshold, the stimulus must be placed at the bottom of the staircase where rod density is highest (21° in nasal retina) (Curcio et al., 1990) and light sensitivity is maximum (about 20° eccentricity) (Aguilar & Stiles, 1954). Moving the dim retinal image closer to the fovea is counterproductive because that would reduce rod density and increase ganglion cell density, thus reducing the number of rods available per ganglion cell for detecting the stimulus. Thus, to maintain visibility of the target the agent remains at the bottom of the staircase; however, when retinal illuminance rises above the rod threshold, the loss of visibility associated with moving the stimulus closer to the fovea is compensated by more available light. The agent can then begin to climb the acuity staircase. With each step increase in retinal illuminance, the stimulus can rise to the next retinal locus where acuity is higher because of greater sampling density. In short, as retinal illuminance rises from the rod threshold to the cone threshold, the agent climbs the scotopic staircase carrying the stimulus from a peripheral location of maximum sensitivity but poor acuity to the foveal location of maximum acuity but poor sensitivity.

The preceding argument that more light makes better sight because extra light enables placing a scotopic stimulus on a less-sensitive retinal location with higher sampling density may also apply to foveal and parafoveal vision of mesopic stimuli. For example, the curved acuity function for foveal stimulation in Figures 9 and 10 may be the envelope of a family of sampling-limited parafoveal functions, which could account for the twofold decline in foveal acuity we measured across the mesopic range. As retinal illuminance falls, the target will eventually become invisible to the rod-free foveola at the cone threshold. Because our stimulus diameter (1.5°) nearly matches the foveola diameter (1.25°), stimulus visibility would improve near the cone threshold by a slight displacement of the stimulus to recruit some rod input to ganglion cells. As argued above, this visibility requirement is a force driving stimulus location up the rod density gradient but down the ganglion-cell density gradient. For example, placing the stimulus just outside the rod-free foveola (but still inside the fovea) would center the stimulus at 1.5° of eccentricity where cone density and rod density are equal (Curcio et al., 1990). Cone density at 1.5° is fourfold less than at 0° eccentricity, which reduces the retinal Nyquist frequency by half (Wilkinson et al., 2016), which is consistent with the twofold decline in foveal acuity reported in Figure 9.

Future experiments with smaller stimuli delivered to known retinal locations with gaze-contingent technology that does not rely on voluntary fixation (Intoy & Rucci, 2020; Ratnam, Domdei, Harmening, & Roorda, 2017) and employing more closely spaced steps in eccentricity would be useful for testing the hypotheses presented above. The basic premise of our experimental method was that insight into the classical, free-viewing condition could be achieved by measuring acuity for stimuli confined to a small, homogeneous patch of retina at known eccentricity. Unfortunately, the smallest patch of retina our equipment could stimulate was 1.5° in diameter, which is relatively large compared to the steep gradient in photoreceptor density and ganglion cell density near the human fovea (Curcio et al., 1990). A similar limitation existed in the study by Kerr (1971), which is the only previous report we are aware of that used a fixed-eccentricity paradigm. As shown in Figure 11, the shapes of Kerr's

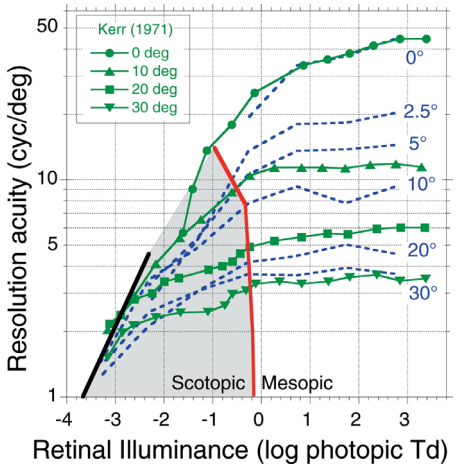

Figure 11. Comparison of current results (dashed blue lines) with those published by Kerr (1971; figure 3, subject JK). Kerr's values of target luminance were converted to retinal illuminance by assuming pupil diameter = 3.5 mm (Watson & Yellott, 2012). To better draw a comparison between the form of the two datasets, we shifted all of Kerr's curves to the left by 0.7 log Td, which might reflect methodological differences mentioned in the text.

functions for a 3° stimulus diameter are remarkably similar to ours despite differences in methodology (Kerr used a dual-staircase paradigm to measure acuity along the horizontal nasal field using brief flashes). Her puzzling finding that scotopic acuity could be measured for foveal fixation may simply be due to the fact that her stimulus was large enough to extend beyond the rod-free foveola to enable resolution of the scotopic target by shifting attention to that portion of the stimulus driving rods. If these conjectures are true, then the stairstep model explains why more light makes better sight even for mesopic vision in the central visual field.

The stairstep model may also provide a mechanistic basis for the clinical use of scotopic acuity as a measure of low-luminance visual dysfunction for monitoring progression of retinal diseases such as age-related macular degeneration (AMD) (Sunness, Rubin, Broman, Applegate, Bressler, & Hawkins, 2008). In this disease, the selective vulnerability of rod photoreceptors is manifest as delayed, rod-mediated dark adaptation and visual dysfunction in general under scotopic conditions (Curcio et al., 2020). Assuming that compromised rods produce weak neural responses, AMD will have a similar effect as reduced retinal illumination; that is, the patient will be forced to depend on more eccentric retina to regain light sensitivity lost to disease. This change in eccentricity will produce a concomitant loss of scotopic acuity that might be useful for monitoring progression of the disease.

Our suggestion that the main effect of retinal illumination on acuity is due to changes in optimum retinal locus is based in part on the close agreement in Figure 10 between the envelope of our constant-eccentricity curves with the cutoff spatial frequency of classic contrast sensitivity functions measured at various retinal illuminances. More generally, we have no reason to suppose this strategy of optimizing retinal locus is employed only for cutoff spatial frequency, which leads us to suggest the following interpretation of classic studies of the effect of retinal illuminance on the contrast sensitivity function (van Meeteren & Vos, 1972; Van Nes & Bouman, 1967). Perhaps the variation of contrast sensitivity with illuminance measured for a given spatial frequency was actually the envelope of a family of sensitivity functions associated with different eccentricities. If so, those classic sensitivity functions represent the optimum detection performance achievable for that frequency when eccentricity is optimized, which might account for major differences compared to contrast sensitivity functions obtained at a fixed retinal eccentricity (Thibos et al., 1996). Such an interpretation has implications for phenomenological models of vision based on published data (Rovamo, Mustonen, & Nasanen, 1994) and on the applications of those models to clinical and basic visual science (Hastings, Marsack, Thibos, & Applegate, 2020; Xu, Wang, Thibos, & Bradley, 2017).

Retinal limits to scotopic and mesopic resolution of gratings

The main purpose of our study was to gather behavioral data that would enable testing of hypotheses about the neuro-anatomical limits to spatial resolution at various levels of retinal illuminance in different parts of the visual field. For mesopic levels of illumination, our data support our previous conclusion that grating acuity in central retina is limited by the density of either ON or OFF midget retinal ganglion cells (the 50% model) or by the combined ON+OFF population (the 100% model) in more peripheral areas of the visual field (Wilkinson et al., 2016). That conclusion is evident in Figure 12 based on the close agreement of mesopic acuity with the Nyquist spatial frequency of the midget (P-cell) pathway (shown by the gray area) calculated from Watson's formula (Watson, 2014) based on the anatomical data of Curcio and Allen (1990). Note that, in this figure, acuity values less than 2 cpd have been corrected by a factor of $(N + 1)/N$, where N is the number of grating cycles displayed in the stimulus, to take account of the spectral dispersion caused by finite windowing of the grating (Anderson et al., 1996). The upper and lower bounds of the gray Nyquist area are the predictions for the 100% and 50% models,

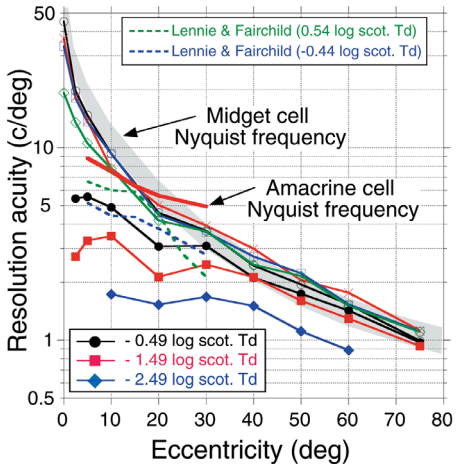

Figure 12. Comparison of current results with those from Lennie and Fairchild (1994) and with anatomical predictions of Nyquist frequencies. The symbol key is the same as in Figure 2, with closed and open symbols indicating mesopic and scotopic acuity, respectively. (For clarity, data for +2.73 and +1.73 log photopic Td are omitted). Acuity values less than 2 cpd have been corrected by a factor of $(N + 1)/N$, where N is the number of grating cycles displayed in the stimulus. The Nyquist frequency for midget ganglion cells is shown by the shaded gray area, for which the upper border represents the 100% model and the lower border represents the 50% model described by Wilkinson et al. (2016). The Nyquist frequency for the A-II amacrine cell population is from Lee et al. (2019).

respectively. Accordingly, vertical cross-sections of the gray area are everywhere the same length ($\sqrt{2}$) when plotted on a logarithmic axis. For eccentricities up to 20°, mesopic acuity agrees more closely with the 50% model, suggesting that neighboring ON and OFF cells redundantly sample central retinal locations. However, beyond 20°, mesopic acuity agrees more closely with the 100% model as expected if neighboring ON and OFF cells independently sample slightly different retinal locations and the two arrays are combined by the brain.

For scotopic levels of retinal illumination in peripheral retina beyond about 30° eccentricity, acuity is also well predicted by the Nyquist frequency of the midget cell array. This agreement is consistent with observer's reports of aliasing for scotopic stimuli and the objective evidence of scotopic aliasing presented in Figures 6 and 7. Although mesopic and scotopic acuity beyond 30° appears to be limited by spacing of midget ganglion cells, the signal pathway from rods to ganglion cells is likely different. The primary (π_0) pathway from rods via ON rod bipolars and A-II amacrine cells is slow but relatively more sensitive and dominates from absolute threshold to low mesopic levels, whereas the secondary pathway (π'_0) via cones and cone bipolars is faster but relatively less sensitive and dominates at high mesopic levels (Sharpe, Stockman, & MacLeod, 1989; Stockman, Sharpe, Zrenner, & Nordby, 1991). By that account, there should be no change in peripheral acuity when crossing the boundary between photopic and mesopic vision because both are limited by the density of midget retinal ganglion cells, a prediction left for future experiments to test.

For eccentricities less than about 30°, scotopic acuity falls well below the P-cell Nyquist limit, as reported previously by Lennie and Fairchild (1994) and confirmed by our results in Figure 12. Anatomical evidence suggests that the limit to scotopic acuity in central retina may be limited by the relatively coarse A-II amacrine array (Lee et al., 2019; Mills & Massey, 1999; Wässle et al., 1995), but our behavioral evidence indicates that central scotopic acuity also falls below the amacrine Nyquist limit. Furthermore, this gap between behavioral acuity and the amacrine Nyquist limit grew increasingly wider as retinal illuminance was reduced toward the rod threshold. Moreover, aliasing was not reported by any of our observers for eccentricities between 2.5° and 10° for the three scotopic illumination levels tested (solid symbols in Figure 12), nor was aliasing reported by Lennie and Fairchild's observers. Taken together, this evidence suggests that central scotopic acuity is not limited by the ambiguity of spatial aliasing caused by neural undersampling. Instead, an even lower limit appears to be imposed by neural spatial filtering that attenuates signal strength, thereby preventing the neural image from fully utilizing the veridical bandwidth of the midget cell pathway. Quantum fluctuations might further reduce the signal-to-noise ratio of neural responses weakened by spatial filtering (Banks, Geisler, & Bennett, 1987). Below we consider in more detail the possibility that the postulated neural filtering is due to spatial summation by the receptive fields of the A-II amacrine cells.

The mosaic formed by the receptive fields of retinal ganglion cells initiates the visual process by converting the continuous retinal image into a discrete neural image for transmission along the optic nerve. In theory, this process is mathematically equivalent to spatial filtering (by spatial summation over the receptive field) of the continuous optical image to produce a continuous neural image, which is then point-sampled to produce the discrete neural image (Thibos & Bradley, 1995). This fundamental theorem conceptually simplifies the simultaneous action of sampling and filtering by the neural mosaic into a sequential process of filtering first, followed by sampling. This ordering, in turn, explains why spatial summation by amacrine receptive fields in the rod visual pathway may act as an anti-alias filter for scotopic vision (provided there is sufficient overlap of their receptive fields), just as optical filtering normally prevents neural undersampling in the fovea (Williams, 1985). In the mammalian retina, rod signals

pass through A-II amacrine cells to drive both ON and OFF ganglion cells (Daw, Jensen, & Brunken, 1990); therefore, spatial summation by amacrines will enlarge the receptive field of the ganglion cell. Overlap of these enlarged ganglion cell fields is measured by the coverage factor, computed as the product of receptive field area and cell density. For a simplified mosaic of uniformly sensitive, square receptive fields, coverage is the square of the ratio of receptive field width to their center-to-center spacing. For an archetypal mosaic with receptive fields that provide complete coverage without gaps or overlap, the coverage factor is unity. Of course, neural receptive fields are neither square nor uniformly sensitive, but analysis based on equivalent diameters of graded circular fields indicates that the coverage factor must be greater than three to prevent aliasing (Thibos & Bradley, 1995). Human A-II amacrines meet this criterion according to Lee et al. (2019), who reported a coverage factor of five for anatomical dendritic fields and possibly even larger coverage by physiological receptive fields due to gap junctions between rods and cones.

In summary, we concur with previous studies that have concluded that the A-II cell mosaic, being the coarsest array in the rod pathway, limits scotopic acuity in central retina (Lee et al., 2019; Mills & Massey, 1999; Wässle et al., 1995). However, unlike scotopic vision in periphery and mesopic vision throughout the visual field, the mechanism responsible for limiting scotopic resolution in the central field is not a loss of neural bandwidth for veridical perception caused by undersampling (Wilkinson et al., 2016). Instead, our evidence suggests that scotopic resolution in central retina is limited by spatial filtering (contributed by receptive fields of amacrine cells) that prevents neural images from utilizing the full bandwidth stipulated by the sampling theorem. In other words, the A-II amacrine cells are effectively anti-aliasing filters because the dendritic fields of this coarse array are large and overlap extensively. Amacrine spatial filtering provides an easy explanation for why scotopic acuity at a fixed location in the central visual field improves as retinal illumination increases. As stated succinctly by MacLeod, Chen, and Stockman (1990), "We see better in bright light not because the grain of the neural response is finer, but because the signals are bigger."

Keywords: visual resolution, scotopic vision, mesopic vision, aliasing, neural sampling

Acknowledgments

Supported by a grant from the National Institutes of Health, National Eye Institute (EY05109 to LNT).

Commercial relationships: none.
Corresponding author: Larry N. Thibos.
Email: thibos@indiana.edu.
Address: School of Optometry, Indiana University, Bloomington, IN, USA.

References

Aguilar, M., & Stiles, W. S. (1954). Saturation of the rod mechanism of the retina at high levels of stimulation. *Optica Acta, 1*(1), 59–65.

Anderson, R. S. (1996). The selective effect of optical defocus on detection and resolution acuity in peripheral vision. *Current Eye Research, 15*(3), 351–353.

Anderson, R. S., Evans, D. W., & Thibos, L. N. (1996). Effect of window size on detection acuity and resolution acuity for sinusoidal gratings in central and peripheral vision. *Journal of the Optical Society of America A, 13*(4), 697–706.

Anderson, R. S., & Thibos, L. N. (1999). Sampling limits and critical bandwidth for letter discrimination in peripheral vision. *Journal of the Optical Society of America A, 16*(10), 2334–2342.

Anderson, R. S., Wilkinson, M. O., & Thibos, L. N. (1992). Psychophysical localization of the human visual streak. *Optometry and Visual Science, 69*(3), 171–174.

Banks, M. S., Geisler, W. S., & Bennett, P. J. (1987). The physical limits of grating visibility. *Vision Research, 27*(11), 1915–1924.

Bradley, A., Thibos, L. N., & Still, D. L. (1990). Visual acuity measured with clinical Maxwellian-view systems: Effects of beam entry location. *Optometry and Visual Science, 67*(11), 811–817.

Craik, K. J. W. (1939). The effect of adaptation upon acuity. *British Journal of Psychiatry, 29*, 252–266.

Curcio, C. A., & Allen, K. A. (1990). Topography of ganglion cells in human retina. *Journal of Comparative Neurology, 300*(1), 5–25.

Curcio, C. A., McGwin, G., Jr., Sadda, S. R., Hu, Z., Clark, M. E., & Sloan, K. R., …Owsley, C. (2020). Functionally validated imaging endpoints in the Alabama study on early age-related macular degeneration 2 (ALSTAR2): design and methods. *BMC Ophthalmology, 20*(1), 196.

Curcio, C. A., Sloan, K. R., Kalina, R. E., & Hendrickson, A. E. (1990). Human photoreceptor topography. *Journal of Comparative Neurology, 292*(4), 497–523.

Daw, N. W., Jensen, R. J., & Brunken, W. J. (1990). Rod pathways in mammalian retinae. *Trends in Neurosciences, 13*(3), 110–115.

Evans, D. W., Wang, Y., Haggerty, K. M., & Thibos, L. N. (2010). Effect of sampling array irregularity and window size on the discrimination of sampled gratings. *Vision Research, 50*(1), 20–30.

Halliday, B. L., & Ross, J. E. (1983). Comparison of two interferometers for predicting visual acuity in patients with cataract. *British Journal of Ophthalmology, 67*(5), 273–277.

Hastings, G. D., Marsack, J. D., Thibos, L. N., & Applegate, R. A. (2020). Combining optical and neural components in physiological visual image quality metrics as a function of luminance and age. *Journal of Vision, 20*(7):20, 1–20, https://doi.org/10.1167/JOV.20.7.20.

Hecht, S. (1928). The relation between visual acuity and illumination. *Journal of General Physiology, 11*(3), 255–281.

Hecht, S., Haig, C., & Wald, G. (1935). The dark adaptation of retinal fields of different size and location. *Journal of General Physiology, 19*(2), 321–337.

Intoy, J., & Rucci, M. (2020). Finely tuned eye movements enhance visual acuity. *Nature Communications, 11*(1), 795.

Kerr, J. L. (1971). Visual resolution in the periphery. *Perception & Psychophysics, 9*(3), 375–378.

Koenig, A. (1897). *Die Abhängigkeit der Sehschärfe von der Beluchtungsintensitat. [The dependence of the visual acuity on the lighting intensity]*. Wien, Germany: Sitzungsberichte der Kaiserlichen Akademie der Wissenschaften; 559.

Kolb, H., & Famiglietti, E. V. (1974). Rod and cone pathways in the inner plexiform layer of cat retina. *Science, 186*(4158), 47–49.

Le Grand, Y. (1937). La formation des images retiniennes. Sur un mode de vision eliminant les defauts optiques de l'oeil. *2e Reunion de l'Institut d'Optique*, Paris.

Lee, S. C. S., Martin, P. R., & Grünert, U. (2019). Topography of neurons in the rod pathway of human retina. *Investigative Ophthalmology & Visual Science, 60*(8), 2848–2859.

Lennie, P., & Fairchild, M. D. (1994). Ganglion cell pathways for rod vision. *Vision Research, 34*(4), 477–482.

Lotmar, W. (1972). Use of Moiré fringes for testing visual acuity of the retina. *Applied Optics, 11*(5), 1266–1268.

Lotmar, W. (1980). Apparatus for the measurement of retinal visual acuity by Moiré fringes. *Investigative Ophthalmology & Visual Science, 19*(4), 393–400.

MacLeod, D. I., Chen, B., & Stockman, A. (1990). The quantum efficiency of vision. In C. Blakemore (Ed.), *Vision: Coding and efficiency* (pp. 169–174). Cambridge, UK: Cambridge University Press.

Mayer, T. (1755). Experimenta circa visus aciem. *Commentationes Societatis Regite Scientiarum Gottingensis, 4*, 97–112.

Mills, S. L., & Massey, S. C. (1999). AII amacrine cells limit scotopic acuity in central macaque retina: A confocal analysis of calretinin labeling. *Journal of Comparative Neurology, 411*(1), 19–34.

Osterberg, G. (1935). Topography of the layer of rods and cones in the human retina. *Acta Ophthalmologica*, (Suppl. 6), 1–103.

Ratnam, K., Domdei, N., Harmening, W. M., & Roorda, A. (2017). Benefits of retinal image motion at the limits of spatial vision. *Journal of Vision, 17*(1):30, 1–11, https://doi.org/10.1167/17.1.30.

Ross, H. E., & Murray, D. J. (1996). *E.H. Weber on the tactile senses* (2nd ed.). East Sussex, UK: Erlbaum (UK) Taylor & Francis.

Rovamo, J., Mustonen, J., & Nasanen, R. (1994). Modelling contrast sensitivity as a function of retinal illuminance and grating area. *Vision Research, 34*(10), 1301–1314.

Rushton, W. A. (1965). Visual adaptation. *Proceedings of the Royal Society B: Biological Sciences, 162*, 20–46.

Scheerer, E. (1987). Tobias Mayer–experiments on visual acuity (1755). *Spatial Vision, 2*(2), 81–97.

Sharpe, L. T., Stockman, A., & MacLeod, D. I. (1989). Rod flicker perception: scotopic duality, phase lags and destructive interference. *Vision Research, 29*(11), 1539–1559.

Shlaer, S. (1937). The relation between visual acuity and illumination. *Journal of General Physiology, 21*(2), 165–188.

Stockman, A., & Sharpe, L. T. (2006). Into the twilight zone: The complexities of mesopic vision and luminous efficiency. *Ophthalmic and Physiological Optics, 26*(3), 225–239.

Stockman, A., Sharpe, L. T., Zrenner, E., & Nordby, K. (1991). Slow and fast pathways in the human rod visual system: electrophysiology and psychophysics. *Journal of the Optical Society of America A, 8*(10), 1657–1665.

Sunness, J. S., Rubin, G. S., Broman, A., Applegate, C. A., Bressler, N. M., & Hawkins, B. S. (2008). Low luminance visual dysfunction as a predictor of subsequent visual acuity loss from geographic atrophy in age-related macular degeneration. *Ophthalmology, 115*(9), 1480–1488.

Thibos, L. N. (1990). Optical limitations of the Maxwellian view interferometer. *Applied Optics, 29*(10), 1411–1419.

Thibos, L. N. (1998). Acuity perimetry and the sampling theory of visual resolution. *Optometry and Visual Science, 75*(6), 399–406.

Thibos, L. N. (2020). Retinal image formation and sampling in a three-dimensional world. *Annual Review of Vision Science, 6*, 469–489.

Thibos, L. N., & Bradley, A. (1993). New methods for discriminating neural and optical losses of vision. *Optometry and Visual Science, 70*(4), 279–287.

Thibos, L. N., & Bradley, A. (1995). Modeling off-axis vision – II: The effect of spatial filtering and sampling by retinal neurons. In E. Peli (Ed.), *Vision models for target detection and recognition* (*Vol. 2*, pp. 338–379). Singapore: World Scientific Press.

Thibos, L. N., Still, D. L., & Bradley, A. (1996). Characterization of spatial aliasing and contrast sensitivity in peripheral vision. *Vision Research, 36*(2), 249–258.

Thibos, L. N., Walsh, D. J., & Cheney, F. E. (1987). Vision beyond the resolution limit: Aliasing in the periphery. *Vision Research, 27*(12), 2193–2197.

van Meeteren, A., & Vos, J. J. (1972). Resolution and contrast sensitivity at low luminances. *Vision Research, 12*(5), 825–833.

Van Nes, F. L., & Bouman, M. A. (1967). Spatial modulation transfer in the human eye. *Journal of the Optical Society of America, 57*(3), 401–406.

Walls, G. L. (1943). Factors in human visual resolution. *Journal of the Optical Society of America, 33*(9), 487–505.

Walraven, J., Enroth-Cugell, C., Hood, D. C., MacLeod, D. I. A., & Schnapf, J. L. (1990). The control of visual sensitivity. In L. Spillman, & J. S. Werner (Eds.), *Visual perception. The neurophysiological foundations* (pp. 53–101). San Diego, CA: Academic Press.

Wang, Y., Thibos, L. N., & Bradley, A. (1997). Effects of refractive error on detection acuity and resolution acuity in peripheral vision. *Investigative Ophthalmology & Visual Science, 38*(10), 2134–2143.

Wang, Y. Z., Thibos, L. N., Lopez, N., Salmon, T., & Bradley, A. (1996). Subjective refraction of the peripheral field using contrast detection acuity. *Journal of the American Optometric Association, 67*(10), 584–589.

Wässle, H., Grünert, U., Chun, M. H., & Boycott, B. B. (1995). The rod pathway of the macaque monkey retina: Identification of AII-amacrine cells with antibodies against calretinin. *Journal of Comparative Neurology, 361*(3), 537–551.

Watson, A. B. (2014). A formula for human retinal ganglion cell receptive field density as a function of visual field location. *Journal of Vision, 14*(7):15, 1–17, https://doi.org/10.1167/14.7.15.

Watson, A. B., & Yellott, J. I. (2012). A unified formula for light-adapted pupil size. *Journal of Vision, 12*(10):12, 1–16, https://doi.org/10.1167/12.10.12.

Weber, E. H. (1846). Tastsinn und Gemeingefuhl. In R. Wagner (Ed.), *Handworterbuch der physiologie* (Vol. *III*, pp. 481–588). Brunswick, Germany: Vieweg.

Wilcox, W. W. (1932). The basis of the dependence of visual acuity on illumination. *Proceedings of the National Academy of Sciences, USA, 18*(1), 47–56.

Wilkinson, M. O., Anderson, R. S., Bradley, A., & Thibos, L. N. (2016). Neural bandwidth of veridical perception across the visual field. *Journal of Vision, 16*(2):1, 1–17, https://doi.org/10.1167/16.2.1.

Williams, D. R. (1985). Aliasing in human foveal vision. *Vision Research, 25*(2), 195–205.

Xu, R., Wang, H., Thibos, L. N., & Bradley, A. (2017). Interaction of aberrations, diffraction, and quantal fluctuations determine the impact of pupil size on visual quality. *Journal of the Optical Society of America A, 34*(4), 481–492.